Cranfield

College of Aeronautics Report No. 9004
March 1990

The Performance of 60° Delta Wings: The Effects of Leading Edge Radius on Vortex Flaps and the Wing.

B K Hu and Prof J L Stollery

The Department of Aerodynamics
College of Aeronautics
Cranfield Institute of Technology
Cranfield. Bedford MK43 OAL. England

College of Aeronautics Report No. 9004
March 1990

The Performance of 60° Delta Wings: The Effects of Leading Edge Radius on Vortex Flaps and the Wing.

B K Hu and Prof J L Stollery

The Department of Aerodynamics
College of Aeronautics
Cranfield Institute of Technology
Cranfield. Bedford MK43 OAL. England

ISBN 1 871564 05 0

£8.00

SUMMARY

Low-speed wind tunnel tests were conducted on 60° delta wings. The wings were tested with well rounded and sharp leading edge vortex flaps to estimate the effects of leading edge radius on the aerodynamic performance. The Reynolds number based on root chord was approximately 0.8×10^{6}.

Results indicate that leading edge radius has little effect on the contribution of the vortex flap to lift/drag ratio on the 60° delta wing. The 60° delta wing with a well rounded leading edge and no vortex flap deflection has a higher lift/drag ratio over almost the entire lift coefficient range tested.

NOTATION

AR	Aspect ratio
C	Wing chord
C_D	Drag coefficient
C_{Di}	Lift induced drag coefficient
C_L	Lift coefficient
K	Lift induced drag factor $\left(K = \frac{C_D - C_{DO}}{C_L^2}\right)$
HL	Hinge line
L/D	Lift/Drag ratio
Re	Reynolds number (based on wing centreline chord)
R_{LE}	Leading edge radius
α	Wing angle of attack
α_o	Zero lift angle of attack
LEVF	Leading edge vortex flap
δ_{LEVF}	Leading edge vortex flap deflection measured normal to the hinge line
S_1	Area of delta 1 with LEVF-1
S_2	Area of delta 1 with LEVF-2

1. INTRODUCTION

On most highly swept and delta wings designed for supersonic cruise the leading edge radius is not sufficiently large to prevent flow separation along the leading edge at high angles of attack (e.g., take off, landing, and manoeuvre). This separation results in the formation of a vortex on the upper surface of the wing as shown in Fig.1. The strength of the leading edge vortex is normally sufficient to result in flow reattachment over the wing's upper surface. Furthermore, the low static pressure at the core of the vortex considerably modifies the spanwise pressure distribution and generates a non-linear vortex lift component of the overall lift produced by the wing (Fig. 1). However, it also contributes a drag force due to the rearward inclination of the resulting force vector (Fig. 2A). The loss of attached flow leading edge suction due to the separation along the leading edge further aggravates the drag. The drag penalty associated with the leading edge vortex flow can be reduced in a number of ways.

Increased aerofoil nose radius has a very powerful effect on retarding the development of the leading edge vortex. The leading edge of the wing is well rounded in order to maintain attached leading edge flow and thus to prevent vortex formation. It recovers leading edge suction and results in large reduction in the lift induced drag. But the high zero lift drag penalty caused by a rounded leading edge at supersonic speeds is usually unacceptable.

An alternative solution is to add leading edge camber to the wing by use of conventional leading edge flap (Fig. 2B). It is effective in preventing vortex formation and promoting attached flow conditions. With this configuration lift induced drag is reduced because of the absence of the vortex and because of the leading edge suction resulting from flow acceleration around the flap. However, some lift is lost with the absence of the low pressure under the vortex core. There may also be a reduction in

overall supersonic performance of the aircraft due to the added weight of a complex flap system.

A leading edge vortex flap (LEVF) can substantially reduce the lift induced drag by 'capturing' the leading edge vortex along a forward facing deflected surface. The vortex suction acting on the surface can develop a thrust. When the flow reattaches at the LEVF hinge line, an attached lifting flow is provided over the upper surface of the wing. This concept is illustrated in Fig. 2C where the flap angle must be such that the flow separates at the edge of the flap and a vortex results. The size of the flap must be sufficient to give reattachment near the LEVF hinge line.

The primary purpose of this paper is:

a) to estimate the effects of leading edge radius on the aerodynamic performance of a LEVF on a 60° delta wing

b) to estimate the effects of leading edge shape on the aerodynamic performance of 60° delta wings.

A series of tests were made in the Cranfield 1A open-jet, low-speed wind tunnel using 60° delta wings made from wood.

2. EXPERIMENTAL DETAILS

Details of the models are given in Fig. 3. The models tested have a leading edge sweep angle of 60° and no camber. The delta 1 model (Fig. 3a) having a symmetric aerofoil section has a thickness/chord ratio of 10% which occurs at 35% C and a well rounded leading edge, R_{LE} = 0.69% C. The spanwise thickness distribution varies linearly from root to tip. The model incorporated a LEVF-1 hinge line running along a ray from the apex to the 75% semispan station at the trailing edge (Fig. 3b). Adding the thin strip to the leading edge of LEVF-1 made a sharp leading edge LEVF-2 (Fig. 3c). The delta 2 model (Fig. 3d) is a

flat delta wing with sharp leading and trailing edges to enhance flow separation. The model also incorporated a LEVF hinge line running along a ray from the apex to the 75% semispan station at the trailing edge (Fig. 3e). All the LEVF deflections were 30° measured in the plan normal to the hinge line.

Measurements of lift and drag were made in the 40" x 27" low-speed open-jet wind tunnel, using a T.E.M. three component wind tunnel balance. All the tests were conducted at a tunnel speed of about 28m/s. The angle of attack range was from -6° to $+ 40^{\circ}$ to include the stall. The Reynolds numbers based on centreline chord were 0.735×10^{6} (delta 1 model) and 0.853×10^{6} (delta 2 model).

The model was mounted on twin shielded struts with a tailsting for angle of attack control (Fig. 4).

Prior to testing, the T.E.M. balance was calibrated. Corrections to the collected data were applied as follows:

A correction to the measured angles of attack due to the constraint of the working section boundaries. This is known as the lift effect and is calculated using the method of images (see Ref. 1).

Owing to the angle of attack correction, the lift vector is inclined and so a correction to the measured drag is also required.

Interference between the twin shielded struts and the wing was assumed negligible.

All the force data have been reduced to coefficient form. These coefficients are based on total plan area. Measured angles of attack, lift and drag coefficients along with the corrected values are presented in tables 1 - 5.

3. RESULTS AND DISCUSSION

According to NACA Langley fully-scale wind tunnel tests on a German Glider in 1946 (see Ref. 9), the vortex lift on a delta wing with thick, blunt leading edges can be significantly increased by forcing separation at the leading edge by adding a thin spanwise leading edge strip.

3.1 Lift

The C_L - α curves are plotted in Figs. 5a and 6a.

Fig. 5a shows that at all angles of attack tested the delta 1 produces markedly higher values of C_L than the delta 1 with LEVFs deflected 30°. The delta 1 stalls at an angles of attack of 30°, while the delta 1 with both LEVF-1 and LEVF-2 do not stall until an angle of attack of 36.6°.

The C_L - α curve also shows a reduced slope for delta 1 with LEVFs deflected 30°. This is due to three effects, a reduction in the projected planform area (whereas the C_L plotted is based on the constant total plan area), a reduction in the effective aspect ratio and a increase in zero lift angles of attack (α_o = 6°, 6.8° for the delta 1 with LEVF-1 and with LEVF-2 respectively).

Fig. 6a shows that the LEVFs deflected 30° on both delta 1 and delta 2 reduce lift. The flat sharp edge delta 2 with LEVF deflected 30° produces higher values of C_L and lift curve slope than the delta 1 with LEVFs deflected 30°.

3.2 Drag

The C_D - α curves are plotted in Figs. 5b and 6b.

Fig. 5b shows that when the LEVF-1 and the LEVF-2 are deflected 30° the angle of attack at which the drag is a minimum will

increase. It moves from about 0.4° to about 8°. At $\alpha < 6^\circ$ the delta 1 with LEVFs deflected 30° produce higher drag than the delta 1. This is because at low angles of attack with the flaps deflected a vortex will form on the lower surface of the flaps. The suction acting on the underside of the flaps will produce negative lift and increased drag. For $\alpha > 6^\circ$ deflecting the LEVFs markedly reduces drag.

Fig. 5b also shows that at $4^\circ < \alpha < 18^\circ$ the drag for a given angle of attack is the same for the delta 1 with either LEVF-1 or LEVF-2 deflected 30°. The well rounded leading edge LEVF-1 probably maintains attached leading edge flow. According to Ref. 2 as the wing angles of attack is increased, a value is reached for which the flow comes smoothly onto the leading edge of the LEVF-2 deflected 30°. There is attached leading edge flow and no flow separation. At $\alpha > 18^\circ$ the LEVF-1 probably continues to maintain attached leading edge flow and leading edge suction acting on LEVF-1 develops a thrust. But the thin leading edge strip of LEVF-2 forces leading edge separation and forms a vortex which spills off the LEVF-2 and is shed over the wing. So the LEVF-2 produces higher drag than the LEVF-1 for the range of angles of attack.

Fig. 6b shows that the delta 1 produces lower drag than the sharp leading edge delta 2 at all angles of attack below 34° This is because the delta 1 with a well rounded leading edge recovers leading edge suction resulting from flow acceleration around the leading edge.

Fig. 6b also shows that the delta 2 with LEVF deflected 30° produces higher drag than the delta 1 with LEVFs deflected 30°.

The $C_{Di} - C_L$ curves are plotted in Figs. 5c and 6c.

Fig. 5c shows that the delta 1 with LEVF-1 deflected 30° produces lower lift induced drag than the delta 1 with LEVF-2 deflected 30° at $C_L < 0.95$.

Fig. 5c also shows that the delta 1 with deflected LEVFs produce higher lift induced drag than the delta 1 over almost the entire C_L range tested. This is because although the delta 1 with deflected LEVFs produces lower drag at any given angle of attack, it needs higher angles of attack than the delta 1 to obtain a given amount of lift.

Fig. 6c shows that the delta 2 with LEVF deflected 30° produces lower lift induced drag than both delta 1 with LEVF-1 deflected 30° at $C_L < 0.8$ and delta 1 with LEVF-2 deflected 30° over C_L range tested.

Fig. 6c also shows that well rounded leading edge delta 1 produces the lowest lift induced drag over almost the entire C_L range.

Lift induced drag factors K for all the configurations tested are plotted in Fig. 7.

3.3 $^{\text{Lift}}/_{\text{Drag}}$ Ratio

The $^{\text{lift}}/_{\text{drag}}$ ratio is used as a basic aerodynamic performance parameter.

Figs. 8a and 8b illustrate $^{L}/_{D}$ versus C_L on the basic 60° delta wings, the wings with LEVFs configurations tested and the effects of leading edge shape on $^{L}/_{D}$.

Fig. 8a shows that the delta 1 with deflected LEVFs has lower $^{\text{lift}}/_{\text{drag}}$ ratios than the basic delta 1 over almost the entire C_L range tested. Deflecting the LEVFs reduces both lift and drag.

Fig. 8a also shows that the delta 1 with LEVF-1 deflected 30° has slightly higher $^{\text{lift}}/_{\text{drag}}$ ratio at $0.15 < C_L \leq 0.6$ and markedly higher $^{\text{lift}}/_{\text{drag}}$ ratio at $0.6 < C_L < 0.95$ than the delta 1 with LEVF-2 deflected 30°

Fig. 8b shows that the delta 1 with the leading edge radius R_{LE} = 0.69% C has the highest $^{lift}/_{drag}$ ratio for all the configurations tested over almost the entire C_L range. The delta 2 with LEVF deflected 30° has higher $^{lift}/_{drag}$ ratio than the flat delta 2. Deflecting the LEVF reduces both lift and drag but the drag reduction is the more significant on the sharp edged flat 60° delta wing.

4. CONCLUSIONS

It must be remembered that all these tests were made at the modest Reynolds number of 0.8×10^6 based on root chord. The effect of Reynolds number on round leading edge delta wings is known to be large.

1. Deflecting the round nose of delta wing 1 reduced both the lift and the drag at a given incidence. Unfortunately the L/D ratio was also reduced.

2. Sharpening the leading edge flap by fitting a thin strip protruding horizontally from the round leading edge had little effect, the performance changes were very similar to those obtained by deflecting the round nose flap.

3. The sequence in which the tests were made has so far precluded tests on the delta 1 wing with the leading edge sharpened but undeflected.

4. Delta wing 2, which had sharp leading edges but a different aerofoil section, was tested. Deflecting the leading edge of this model decreased C_L and C_D but increased the $^{lift}/_{drag}$ ratio.

5. Of all the configurations tested the best L/D ratios were measured on the round nosed delta 1 model with no flap deflection.

REFERENCES

1. Parkhurst, R.C., and Holder, D.W. Wind tunnel technique: an account of experimental methods in low- and high-speed wind tunnels. PITMAN, 1952.

2. Stollery, J.L., and Ellis, D.G. The behaviour and performance of vortex flaps. College of Aeronautics Report No. NFP8914, November 1989.

3. Ellis, D.G. The behaviour and performance of leading edge vortex flaps. College of Aeronautics Report No. 8601, 1986.

4. Jones, R., Miles, C.J.W., and Pursey, P.S. Experiments in the compressed air tunnel on swept-back wings including two delta wings. A.R.C. Technical Report R & M No. 2871, 1954.

5. Kulfan, R.M. Wing geometry effects on leading edge vortices. AIAA 79-1872. August 20-22, 1979.

6. Hu, B.K. and Stollery, J.L. The performance of 60° delta wings: the effects of leading edge radius and vortex flaps. College of Aeronautics Report No. 9002, November 1989.

7. Paul L.Coe, Jr., Jarrett K. Huffman, and James W.Fenbert. Leading-edge deflection optimization for a highly swept arrow-wing configuration. NASA TP 1777, December 1980.

8. Pau L.Coe, Jr., and Robert P.Weston. Effects of wing leading-edge deflection on low-speed aerodynamic characteristics of a low-aspect-ratio highly swept arrow-wing configuration. NASA TP 1434, June 1979.

9. Herbert A.Wilson, Jr., and J.Calvin Lovell. Full-scale investigation of the maximum lift and flow characteristics of an airplane having approximately triangular plan form. NACA RM No.L6K20, February 12, 1947.

10. W.Elliott Schoonover, Jr. Wind-tunnel investigation of vortex flaps on a highly swept interceptor configuration. ICAS-82-6.7.3.

Date: 20/9/89 p.m.

TABLE 1

Incidence, lift coefficient, drag coefficient (both corrected and uncorrected) and lift/drag ratio for Delta 1.

NO.	α°		C_L		C_D		$L/D(C)$
	$\alpha_{(U)}$	$\alpha_{(C)}$	$C_{L(U)}$	$C_{L(C)}$	$C_{D(U)}$	$C_{D(C)}$	
1	-6	- 5.630	- 0.248	- 0.248	0.045	0.043	-
2	-4	- 3.756	- 0.164	- 0.164	0.035	0.034	-
3	-2	- 1.890	- 0.074	- 0.074	0.021	0.021	-
4	0	- 0.009	0.006	0.006	0.018	0.018	0.333
5	2	1.855	0.097	0.097	0.020	0.020	4.850
6	4	3.708	0.196	0.196	0.022	0.021	9.333
7	6	(5.508) 5.580	(0.33) 0.282	(0.33) 0.282	(0.033) 0.032	(0.03) 0.030	(11.000) 9.400
8	8	7.382	0.415	0.415	0.046	0.042	9.881
9	10	9.270	0.490	0.490	0.063	0.057	8.596
10	12	11.151	0.570	0.571	0.088	0.080	7.138
11	14	13.033	0.649	0.650	0.117	0.106	6.132
12	16	14.924	0.722	0.723	0.153	0.140	5.164
13	18	16.833	0.783	0.784	0.206	0.190	4.126
14	20	18.762	0.831	0.832	0.252	0.234	3.556
15	22	20.652	0.905	0.906	0.301	0.280	3.236
16	24	22.543	0.978	0.979	0.356	0.331	2.958
17	26	24.434	1.051	1.052	0.407	0.379	2.776
18	28	26.351	1.107	1.108	0.466	0.435	2.547
19	30	28.318	1.129	1.130	0.535	0.502	2.251
20	32	30.300	1.141	1.142	0.583	0.550	2.076
21	34	32.334	1.118	1.119	0.625	0.593	1.887
22	36	34.361	1.100	1.101	0.646	0.615	1.790
23	38	36.477	1.022	1.023	0.656	0.629	1.626
24	40	38.631	0.919	0.920	0.638	0.617	1.491

Date: 19/9/89 p.m.

TABLE 2

Incidence, lift coefficient, drag coefficient (both corrected and uncorrected) and lift/drag ratio for Delta 2.

NO.	α°		C_L		C_D		$L/D_{(C)}$
	$\alpha_{(U)}$	$\alpha_{(C)}$	$C_{L(U)}$	$C_{L(C)}$	$C_{D(U)}$	$C_{D(C)}$	
1	-6	- 5.587	- 0.212	- 0.212	0.060	0.059	-
2	-4	- 3.774	- 0.116	- 0.116	0.048	0.048	-
3	-2	- 1.940	- 0.031	- 0.031	0.034	0.034	-
4	0	- 0.109	0.056	0.056	0.028	0.028	2.000
5	2	1.741	0.133	0.133	0.029	0.028	4.750
6	4	3.569	0.221	0.221	0.032	0.030	7.367
7	6	5.427	0.294	0.294	0.039	0.036	8.167
8	8	7.258	0.381	0.381	0.055	0.050	7.620
9	10	9.073	0.476	0.476	0.075	0.067	7.104
10	12	10.851	0.590	0.591	0.114	0.102	5.794
11	14	12.738	0.648	0.649	0.149	0.135	4.807
12	16	14.568	0.735	0.736	0.186	0.168	4.381
13	18	16.436	0.803	0.804	0.231	0.209	3.847
14	20	18.303	0.871	0.872	0.283	0.257	3.393
15	22	20.179	0.935	0.936	0.343	0.314	2.981
16	24	22.031	1.011	1.012	0.414	0.380	2.663
17	26	23.986	1.034	1.035	0.463	0.427	2.424
18	28	25.898	1.079	1.080	0.528	0.499	2.163
19	30	27.836	1.111	1.112	0.580	0.539	2.063
20	32	29.859	1.099	1.100	0.634	0.594	1.852
21	34	31.939	1.058	1.059	0.665	0.628	1.686
22	36	34.165	0.942	0.943	0.658	0.628	1.502
23	38	36.385	0.829	0.830	0.601	0.578	1.436
24	40	38.453	0.794	0.795	0.597	0.576	1.380

Date: 27/9/89 p.m.

TABLE 3

Incidence, lift coefficient, drag coefficient (both corrected and uncorrected) and lift/drag ratio for Delta 2 with LEVF. $\delta_{LEVF} = 30^{\circ}$.

NO.	α°		C_L		C_D		$L/D_{(C)}$
	$\alpha_{(U)}$	$\alpha_{(C)}$	$C_{L(U)}$	$C_{L(C)}$	$C_{D(U)}$	$C_{D(C)}$	
1	-6	- 5.482	- 0.266	- 0.266	0.069	0.067	-
2	-4	- 3.634	- 0.188	- 0.188	0.051	0.050	-
3	-2	- 1.776	- 0.115	- 0.115	0.039	0.039	-
4	0	0.084	- 0.043	- 0.043	0.033	0.033	-
5	2	1.940	0.031	0.031	0.025	0.025	1.240
6	4	3.776	0.115	0.115	0.027	0.027	4.259
7	6	5.649	0.180	0.180	0.031	0.030	6.000
8	8	7.494	0.260	0.260	0.037	0.035	7.429
9	10	9.347	0.335	0.335	0.044	0.040	8.375
10	12	11.223	0.399	0.399	0.051	0.044	9.068
11	14	13.082	0.471	0.471	0.066	0.059	7.983
12	16	14.940	0.544	0.545	0.088	0.078	6.987
13	18	16.788	0.622	0.623	0.115	0.102	6.108
14	20	18.646	0.695	0.696	0.164	0.148	4.703
15	22	20.516	0.762	0.763	0.209	0.189	4.037
16	24	22.379	0.832	0.833	0.258	0.235	3.545
17	26	24.241	0.903	0.904	0.306	0.278	3.252
18	28	26.130	0.960	0.961	0.362	0.331	2.903
19	30	28.060	0.996	0.997	0.432	0.399	2.499
20	32	30.003	1.025	1.026	0.496	0.461	2.226
21	34	32.013	1.020	1.021	0.553	0.518	1.971
22	36	34.023	1.015	1.016	0.576	0.542	1.875
23	38	36.101	0.975	0.976	0.622	0.590	1.654
24	40	38.175	0.937	0.938	0.608	0.579	1.620

Date: 18/1/90 a.m.

TABLE 4

Incidence, lift coefficient, drag coefficient (both corrected and uncorrected) and lift/drag ratio for Delta 1 with LEVF-1, $\delta_{LEVF} = 30^{\circ}$

NO.	α°		C_L		C_D		$L/_{D(C)}$
	$\alpha_{(U)}$	$\alpha_{(C)}$	$C_{L(U)}$	$C_{L(C)}$	$C_{D(U)}$	$C_{D(C)}$	
1	-6	- 5.332	- 0.448	- 0.448	0.092	0.087	-
2	-4	- 3.449	- 0.370	- 0.370	0.074	0.071	-
3	-2	- 1.569	- 0.289	- 0.289	0.057	0.055	-
4	0	0.317	- 0.213	- 0.213	0.042	0.041	-
5	2	2.317	- 0.142	- 0.142	0.031	0.031	-
6	4	4.095	- 0.064	- 0.064	0.023	0.023	-
7	6	5.985	0.010	0.010	0.021	0.021	0.476
8	8	7.875	0.084	0.084	0.021	0.021	4.000
9	10	9.799	0.135	0.135	0.023	0.023	5.870
10	12	11.702	0.200	0.200	0.027	0.026	7.692
11	14	13.607	0.264	0.264	0.033	0.031	8.516
12	16	15.525	0.319	0.319	0.039	0.036	8.861
13	18	17.438	0.377	0.377	0.049	0.045	8.378
14	20	19.362	0.428	0.428	0.061	0.056	7.643
15	22	21.289	0.477	0.477	0.073	0.067	7.119
16	24	23.209	0.531	0.532	0.094	0.087	6.115
17	26	25.119	0.591	0.592	0.121	0.112	5.286
18	28	27.039	0.645	0.646	0.151	0.140	4.614
19	30	28.963	0.696	0.697	0.184	0.172	4.052
20	32	30.753	0.785	0.786	0.216	0.200	3.930
21	34	32.702	0.871	0.872	0.242	0.223	3.910
22	36	34.637	0.915	0.916	0.294	0.273	3.355
23	38	36.574	0.957	0.958	0.349	0.326	2.939
24	40	38.671	0.950	0.951	0.397	0.377	2.523

Date: 8/3/90 p.m.

TABLE 5

Incidence, lift coefficient, drag coefficient (both corrected and uncorrected) and lift/drag ratio for Delta 1 with LEVF-2 $\delta_{LEVF} = 30^{\circ}$

NO.	α°		C_L		C_D		$L/_{D(C)}$
	$\alpha_{(U)}$	$\alpha_{(C)}$	$C_{L(U)}$	$C_{L(C)}$	$C_{D(U)}$	$C_{D(C)}$	
1	-6	- 5.244	- 0.452	- 0.452	0.107	0.101	-
2	-4	- 3.291	- 0.424	- 0.424	0.090	0.085	-
3	-2	- 1.421	- 0.346	- 0.346	0.073	0.070	-
4	0	0.460	- 0.275	- 0.275	0.055	0.053	-
5	2	2.331	- 0.198	- 0.198	0.038	0.037	-
6	4	4.177	- 0.106	- 0.106	0.026	0.026	-
7	6	6.028	- 0.017	- 0.017	0.019	0.019	-
8	8	7.928	0.043	0.043	0.018	0.018	2.389
9	10	9.808	0.115	0.115	0.022	0.022	5.227
10	12	11.702	0.178	0.178	0.026	0.025	7.120
11	14	13.597	0.241	0.241	0.033	0.031	7.774
12	16	15.493	0.303	0.303	0.038	0.035	8.657
13	18	17.388	0.366	0.366	0.050	0.046	7.957
14	20	19.278	0.432	0.432	0.065	0.060	7.216
15	22	21.139	0.515	0.516	0.090	0.082	6.293
16	24	23.039	0.575	0.576	0.114	0.105	5.486
17	26	24.947	0.630	0.631	0.153	0.142	4.444
18	28	26.831	0.699	0.700	0.189	0.175	4.000
19	30	28.741	0.753	0.754	0.233	0.217	3.475
20	32	30.626	0.822	0.823	0.297	0.278	2.960
21	34	32.549	0.868	0.869	0.353	0.332	2.617
22	36	34.502	0.896	0.897	0.396	0.373	2.405
23	38	36.440	0.933	0.934	0.441	0.416	2.245
24	40	38.443	0.931	0.932	0.476	0.451	2.067

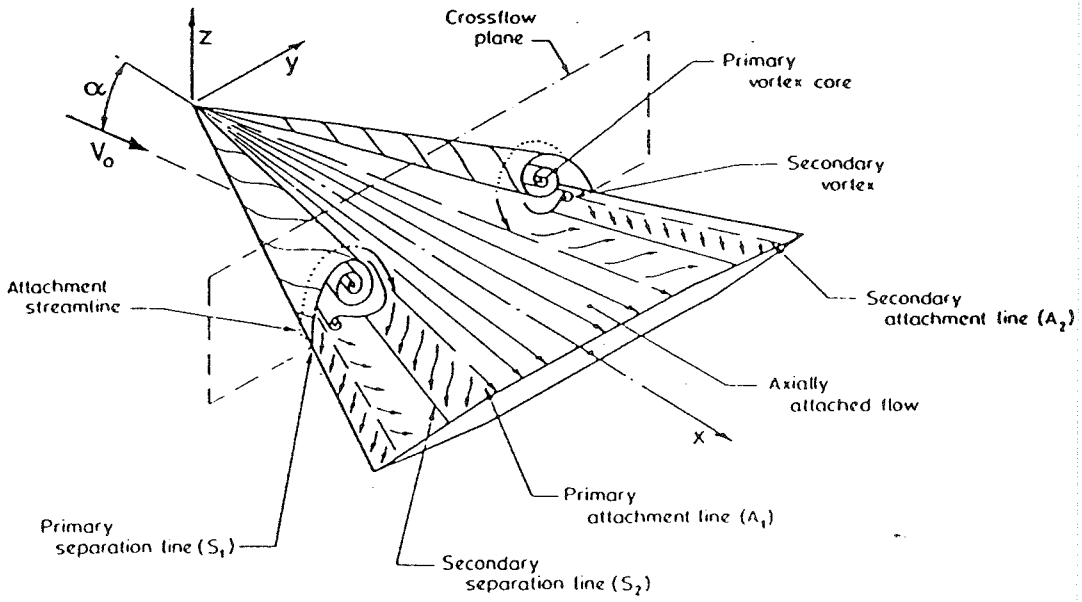

CROSS-FLOW PLANE PRESSURE

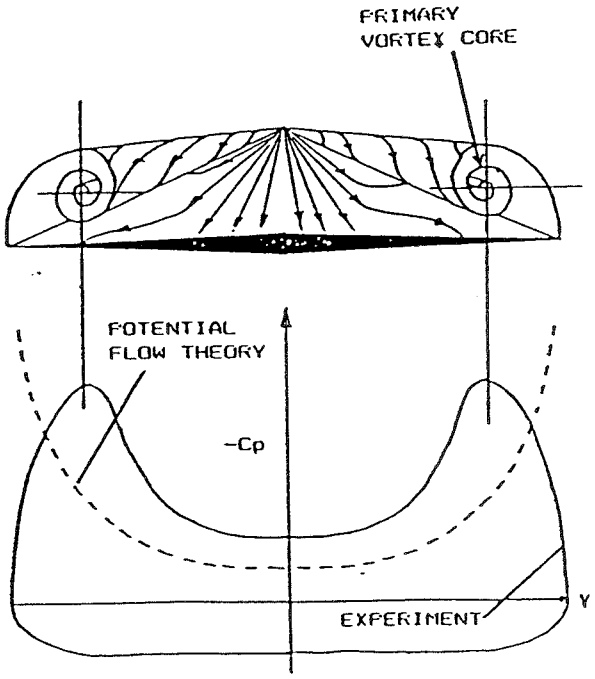

Figure 1. Sharp leading edge delta wing flow pattern

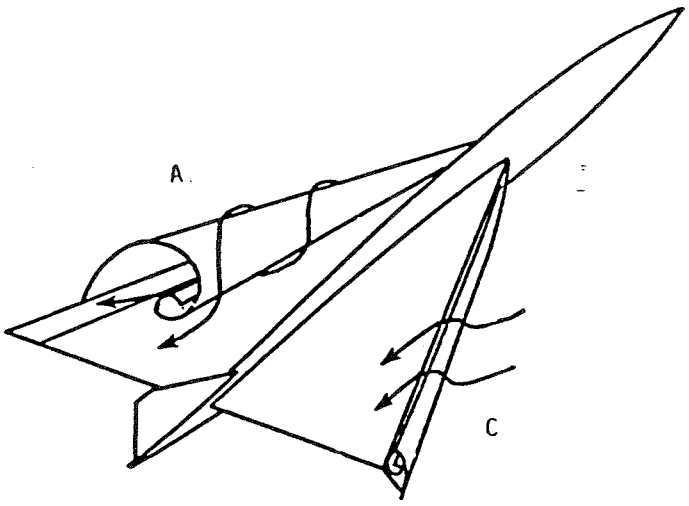

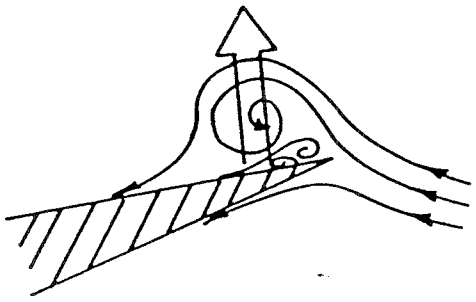

A: VORTEX FORCE ON WING LEADING EDGE

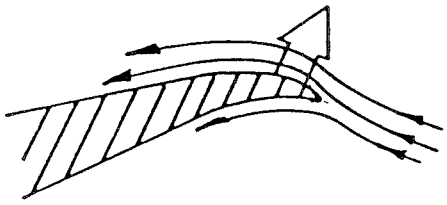

B: FORCE ON CAMBERED LEADING EDGE

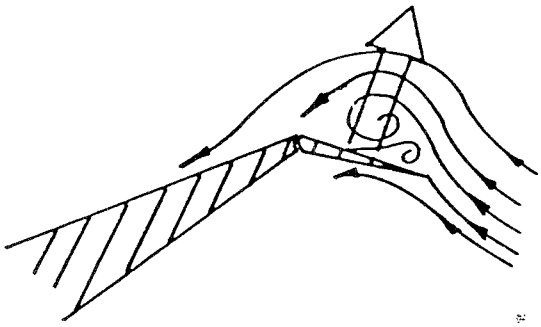

C: FORCE ON VORTEX FLAP

Figure 2. Flows and forces on delta wing leading edges due to different leading edge shapes

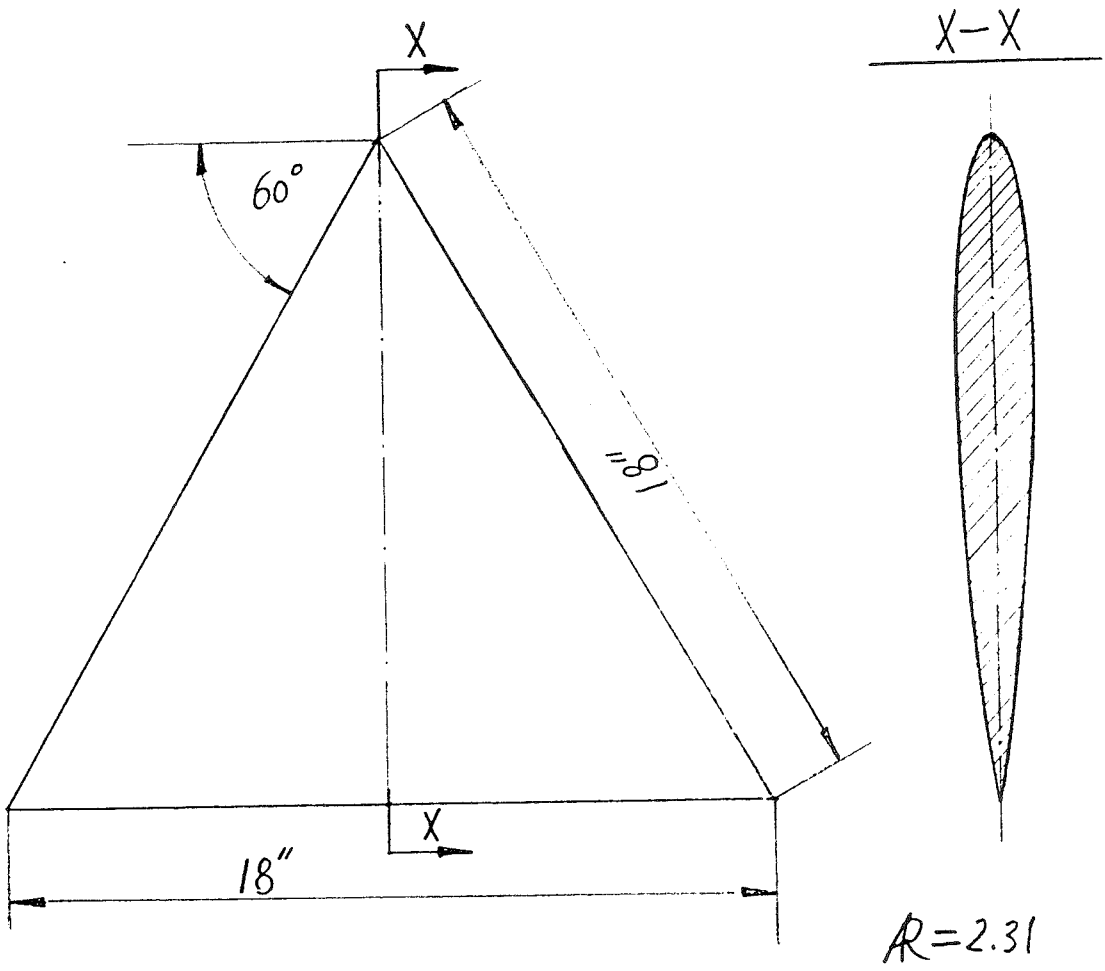

Ordinates of Wing Section in Terms of Chord
(Symmetric aerofoil section)

Distance from leading edge	Height above chord × 100	Distance from leading edge	Height above chord × 100
0	0	0·40	4·96
0·005	0·825	0·45	4·77
0·0075	1·008	0·50	4·49
0·0125	1·300	0·55	4·15
0·025	1·821	0·60	3·75
0·050	2·53	0·65	3·32
0·075	3·04	0·70	2·86
0·100	$3·44_5$	0·75	2·39
0·15	4·05	0·80	1·92
0·20	$4·47_5$	0·85	$1·43_5$
0·25	4·76	0·90	0·95
0·30	$4·93_5$	0·95	0·48
0·35	5·00	1·0	0
		Nose radius = 0·0069 × chord	

Figure 3a. Delta 1 model details

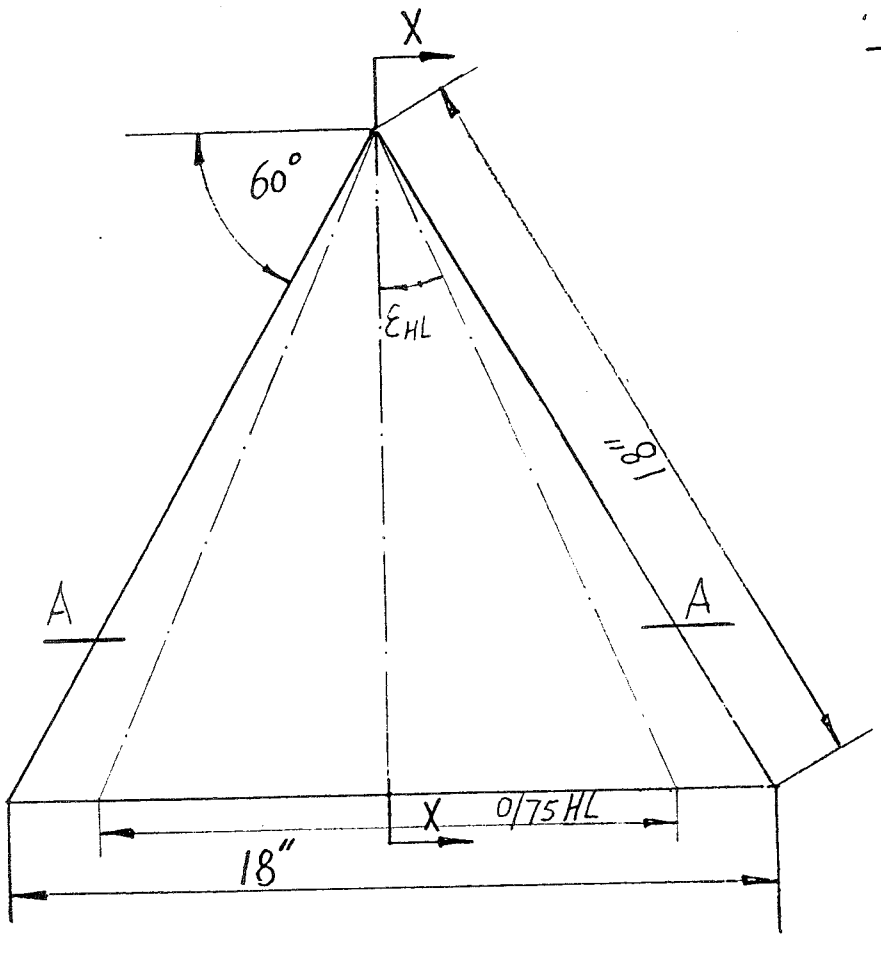

X-X

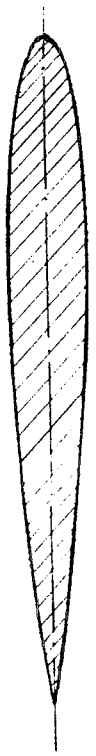

AR=2.31

$S_1 = 0.0905 m^2$

A-A

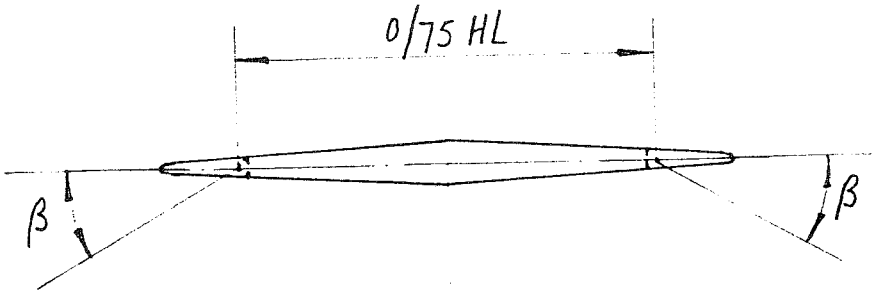

$\delta_{LEF} = 30°$

δ_{LEF} is measured in a plane perpendicular to LEF hinge line.

β is measured in the crossflow plane.

$\beta = \text{Cos } \varepsilon_{HL} \; \delta_{LEF}$

Figure 3b. Delta 1 with LEVF-1 model details

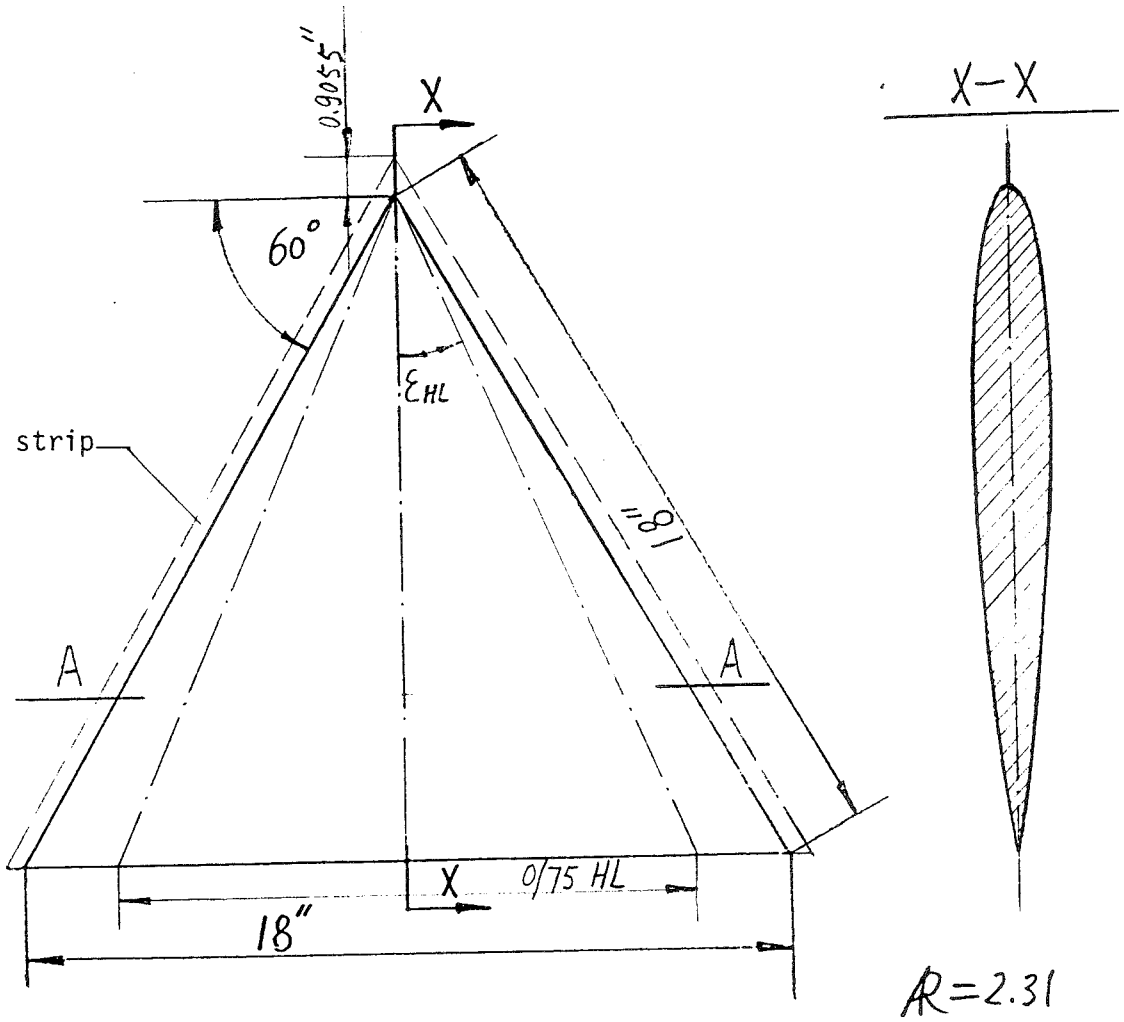

$\delta_{LEVF} = 30^\circ$

δ_{LEVF} is measured in a plane perpendicular to LEVF hinge line.

β is measured in the crossflow plane.

$\beta = \text{Cos } \varepsilon_{HL}\ \delta_{LEVF}$

Figure 3c. Delta 1 with LEVF-2 model details

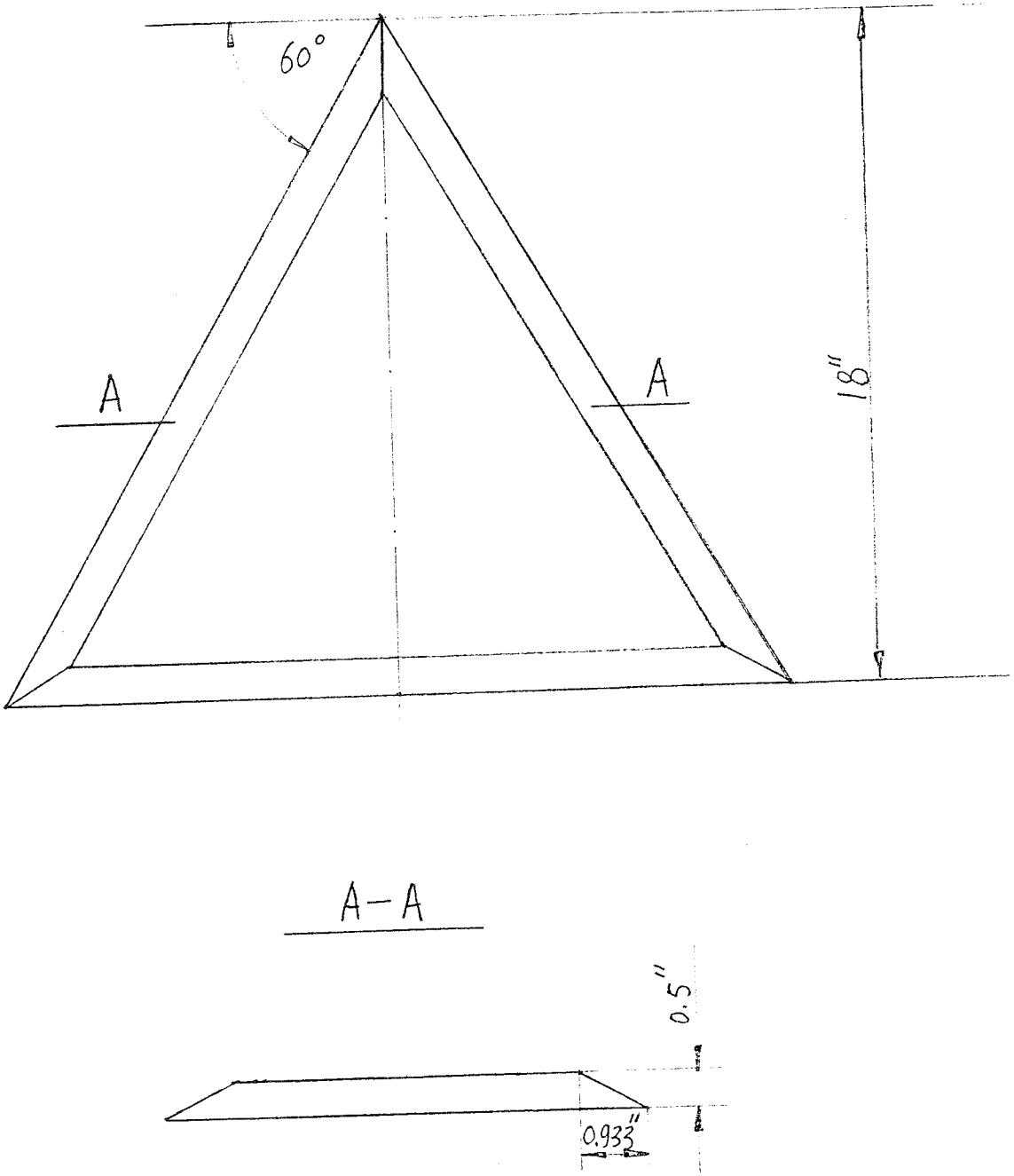

Figure 3d. Delta 2 model details

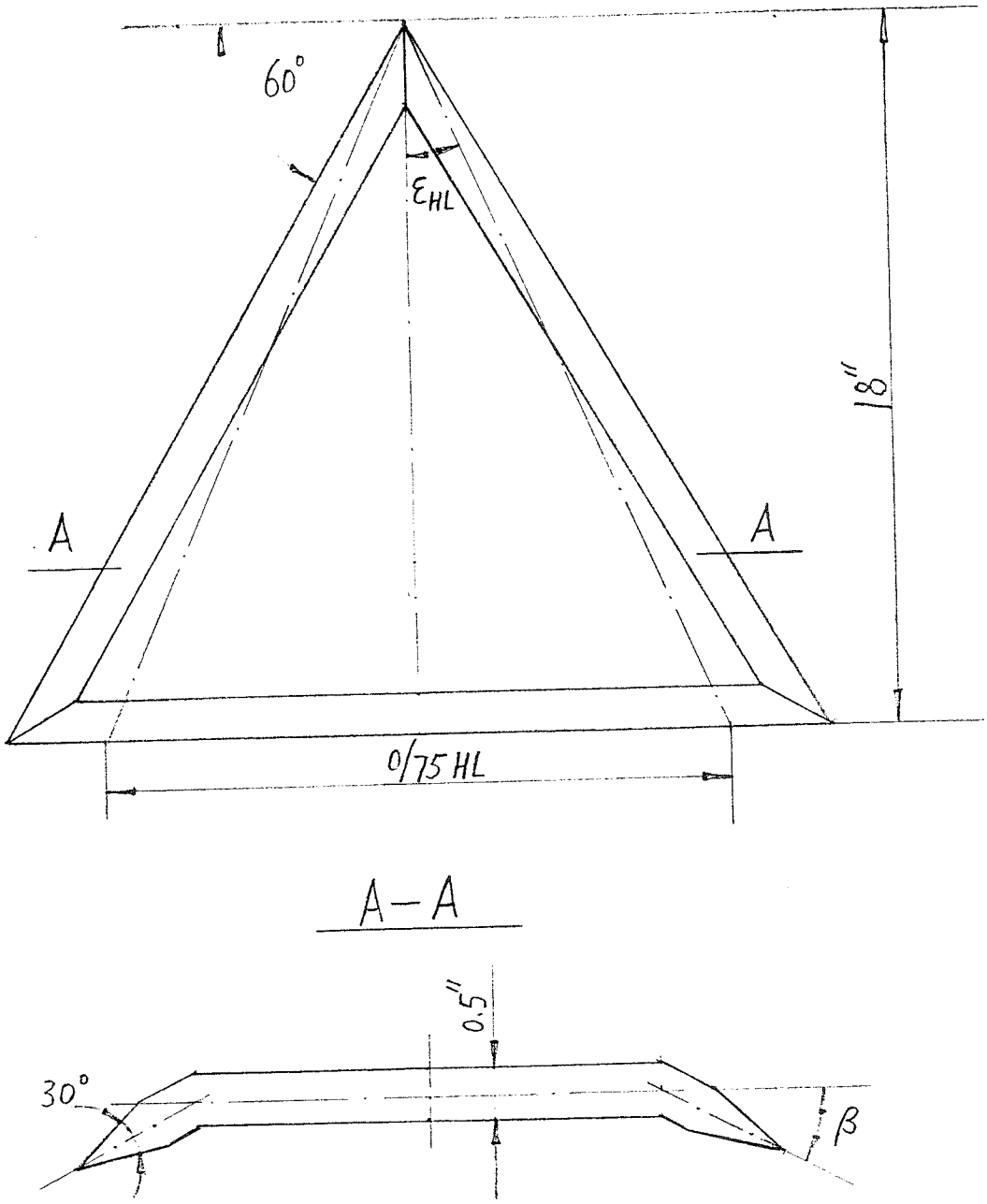

$\delta_{LEVF} = 30^{\circ}$

δ_{LEVF} is measured in a plane perpendicular to LEVF hinge line.

β is measured in the crossflow plane.

$\beta = \text{Cos } \varepsilon_{HL} \; \delta_{LEVF}$

Figure 3e. Delta 2 with LEVF model details

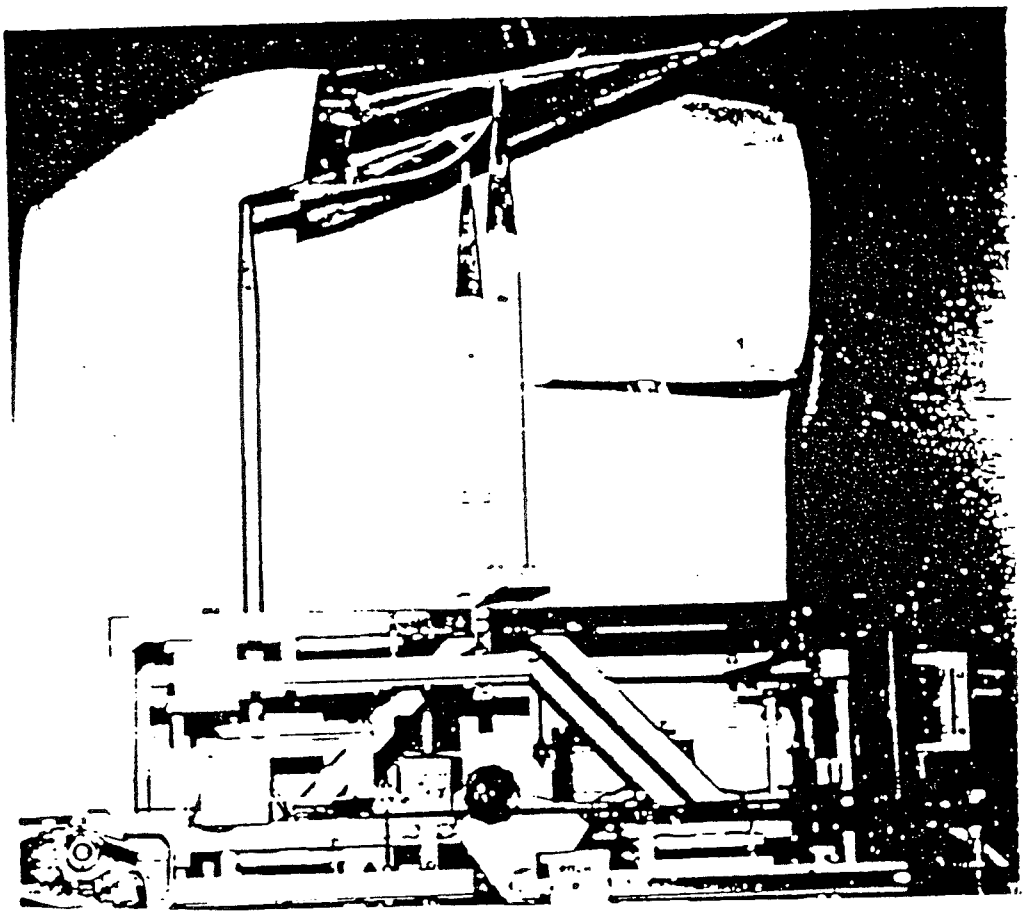

Figure 4. Model mounting and balance

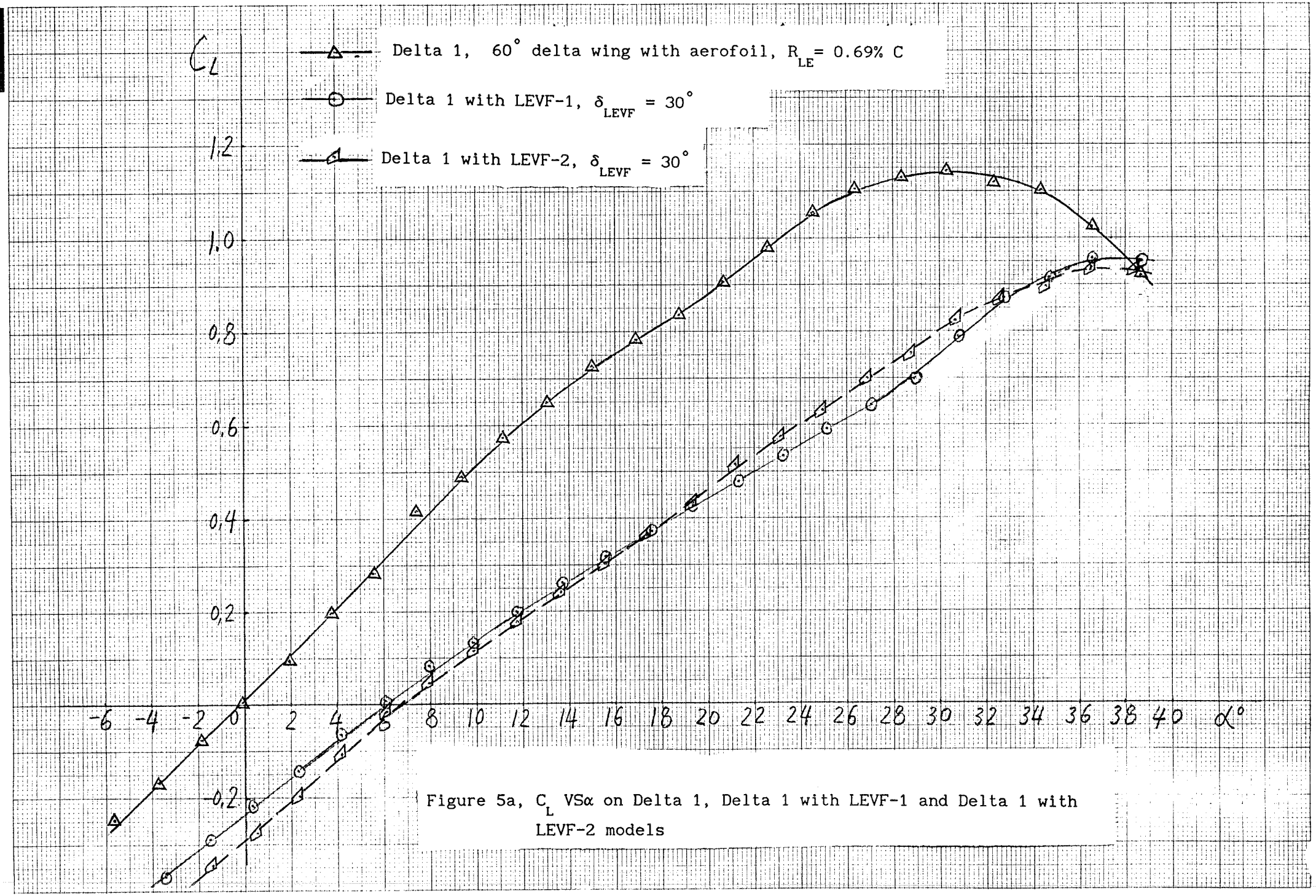

Figure 5a, C_L VSα on Delta 1, Delta 1 with LEVF-1 and Delta 1 with LEVF-2 models

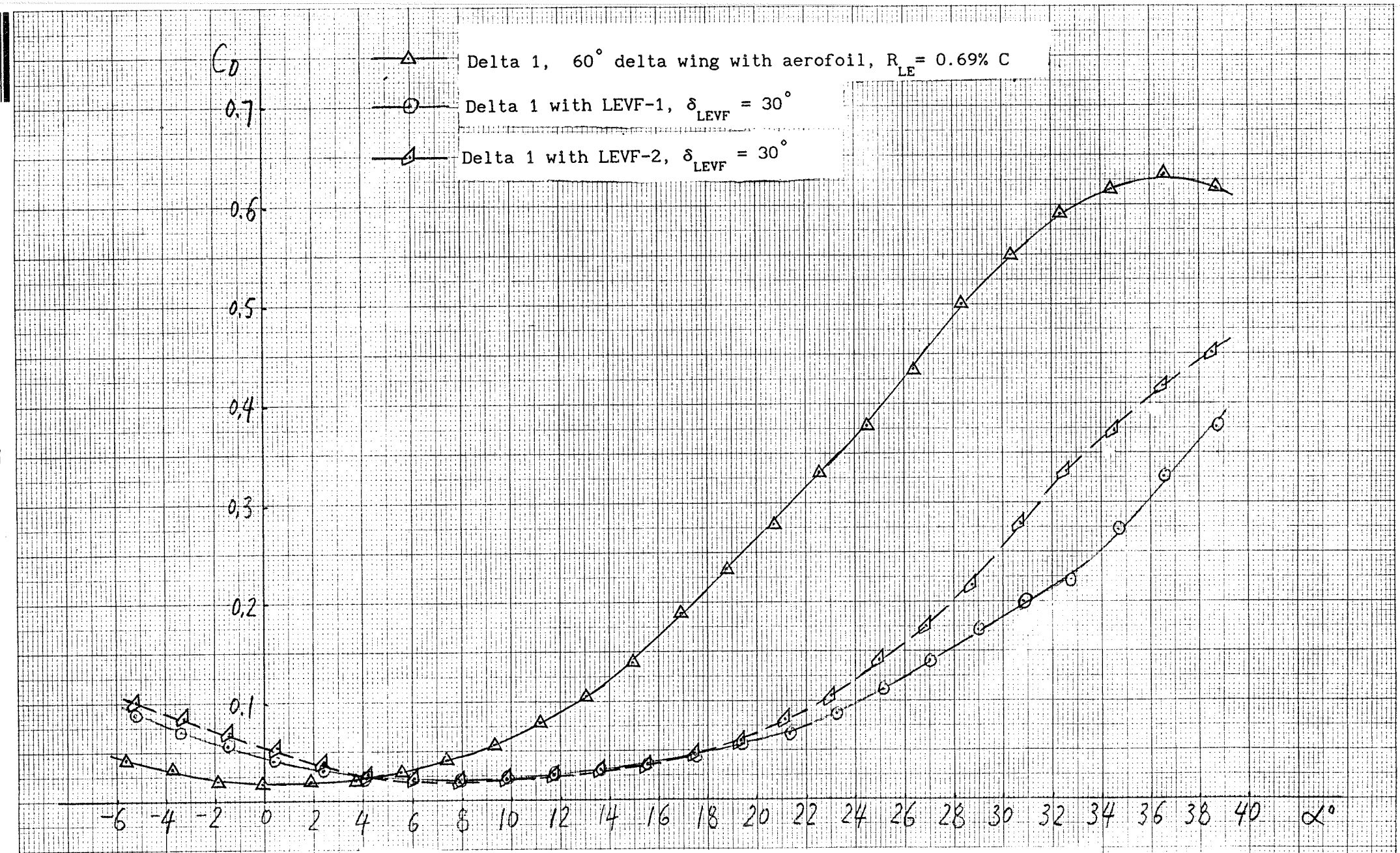

Figure 5b. C_D VS α on Delta 1, Delta 1 with LEVF-1 and Delta 1 with LEVF-2 models

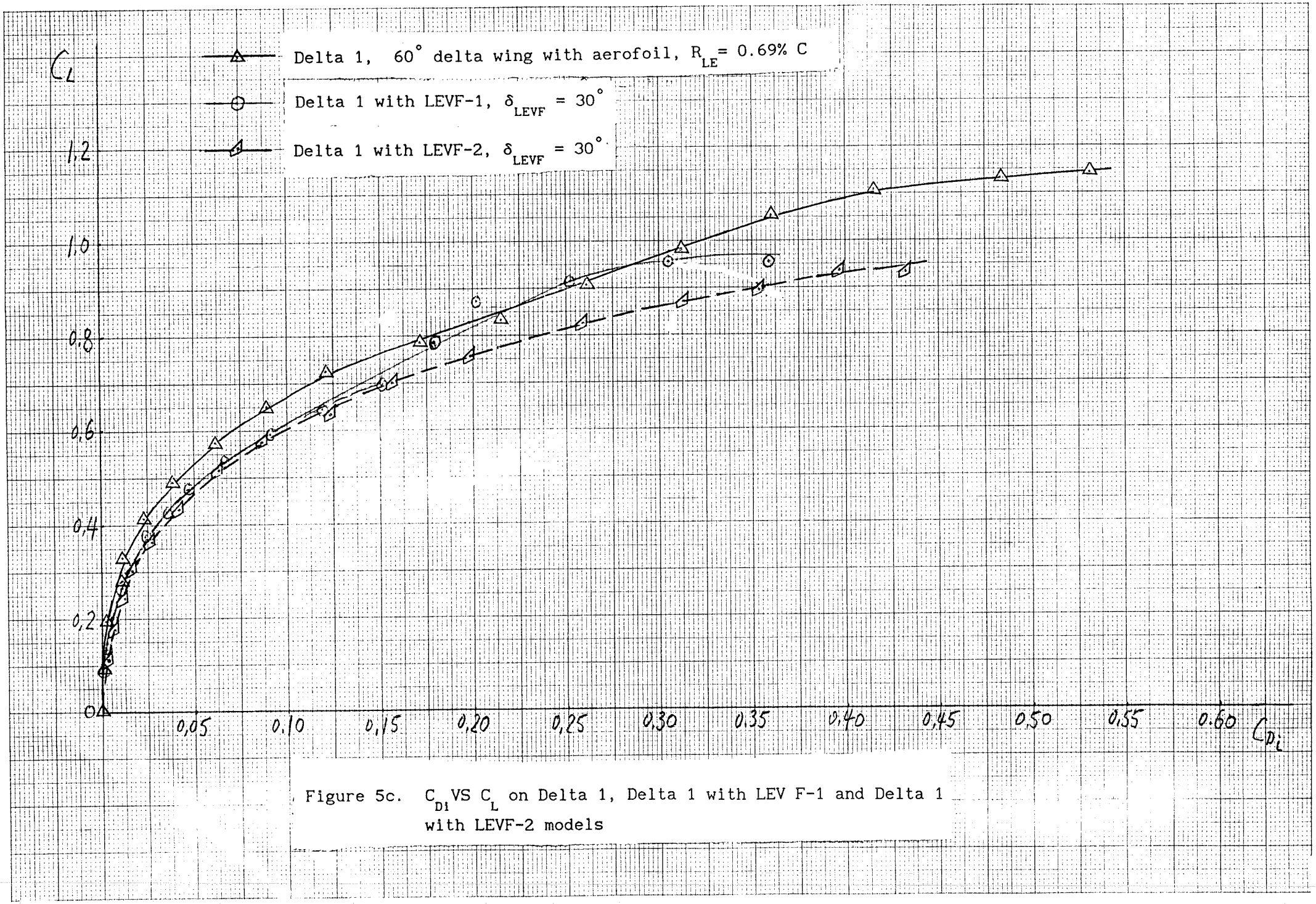

Figure 5c. C_{Di} VS C_L on Delta 1, Delta 1 with LEV F-1 and Delta 1 with LEVF-2 models

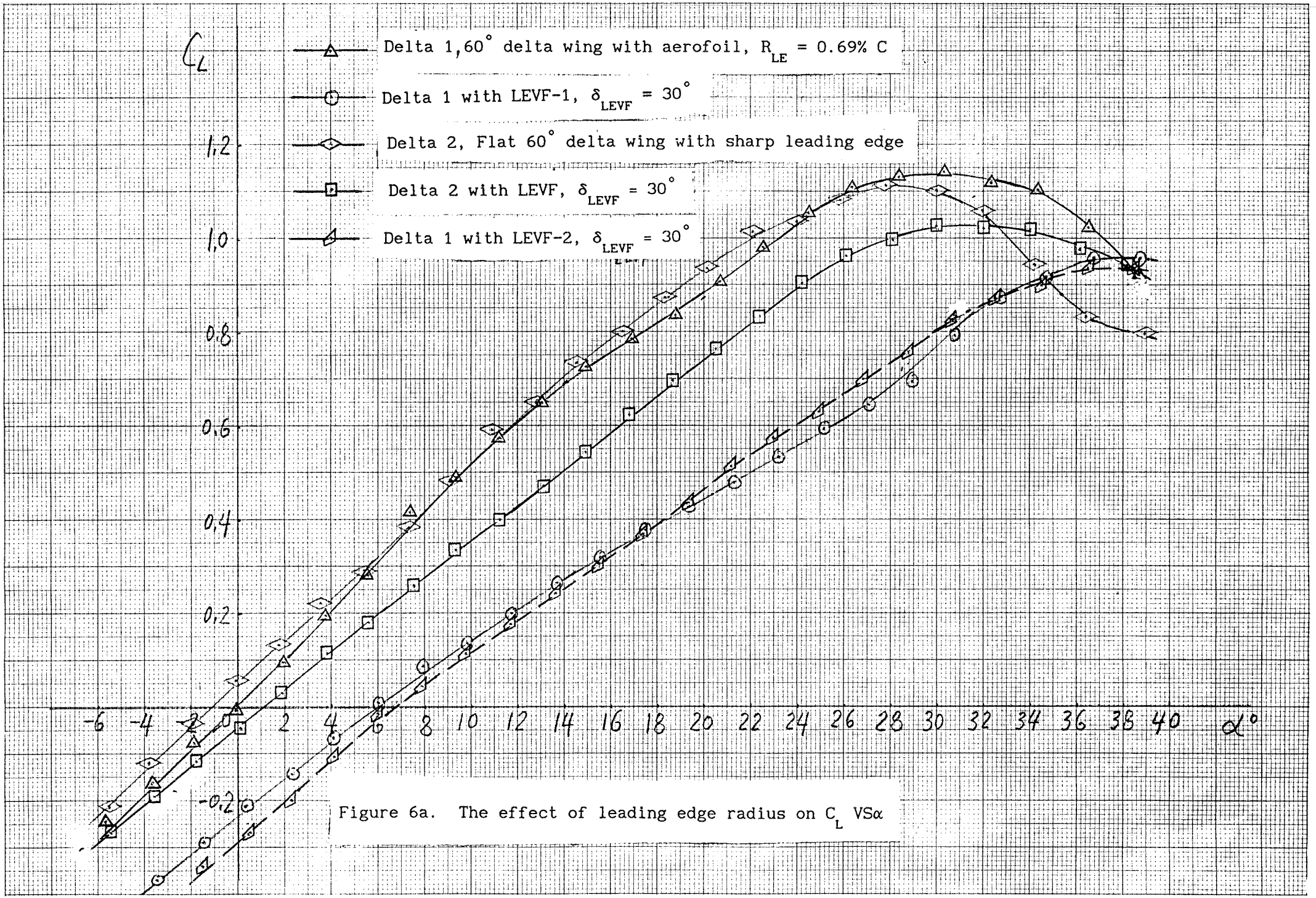

Figure 6a. The effect of leading edge radius on C_L VSα

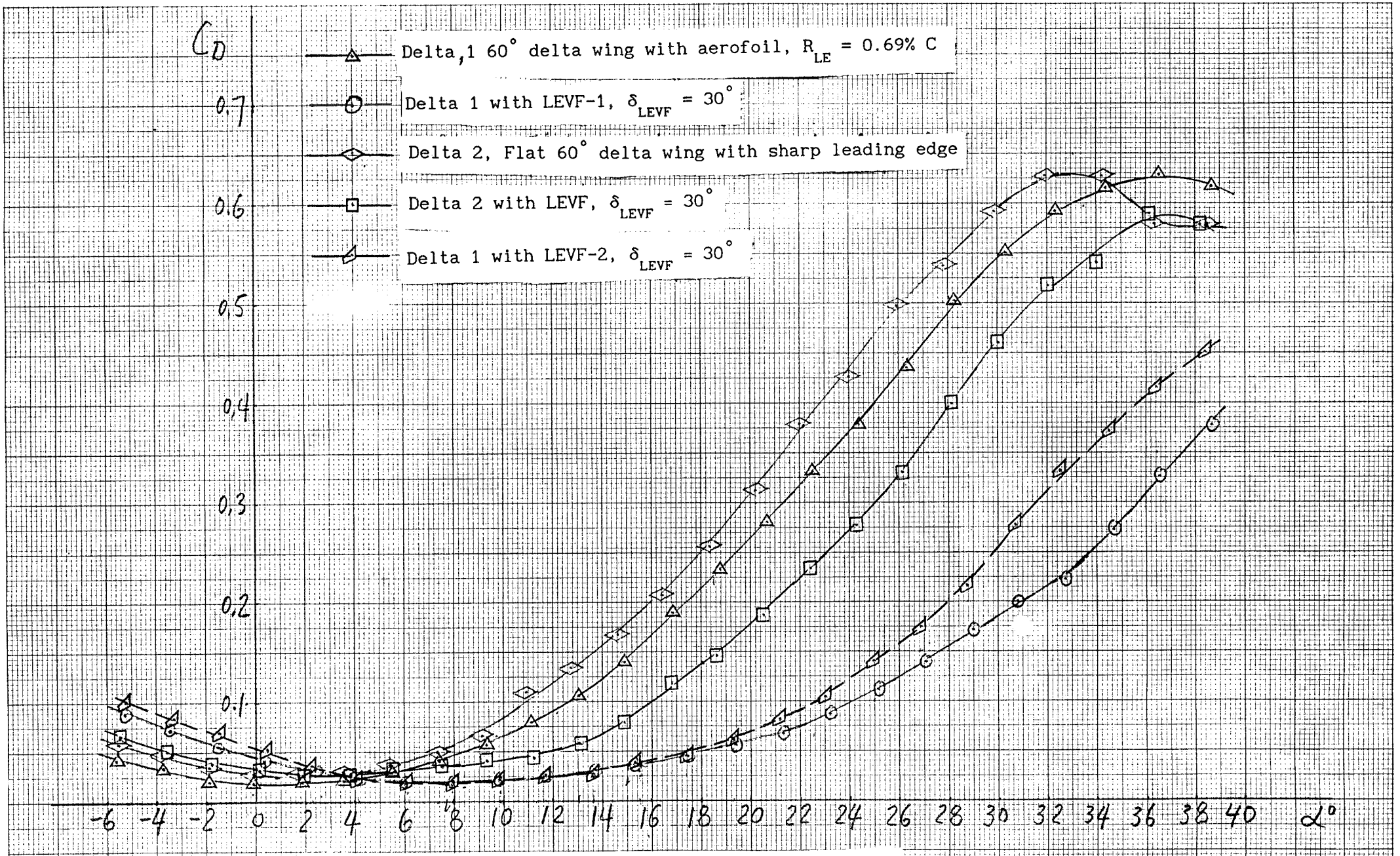

Figure 6b. The effect of leading edge radius on C_D VSα

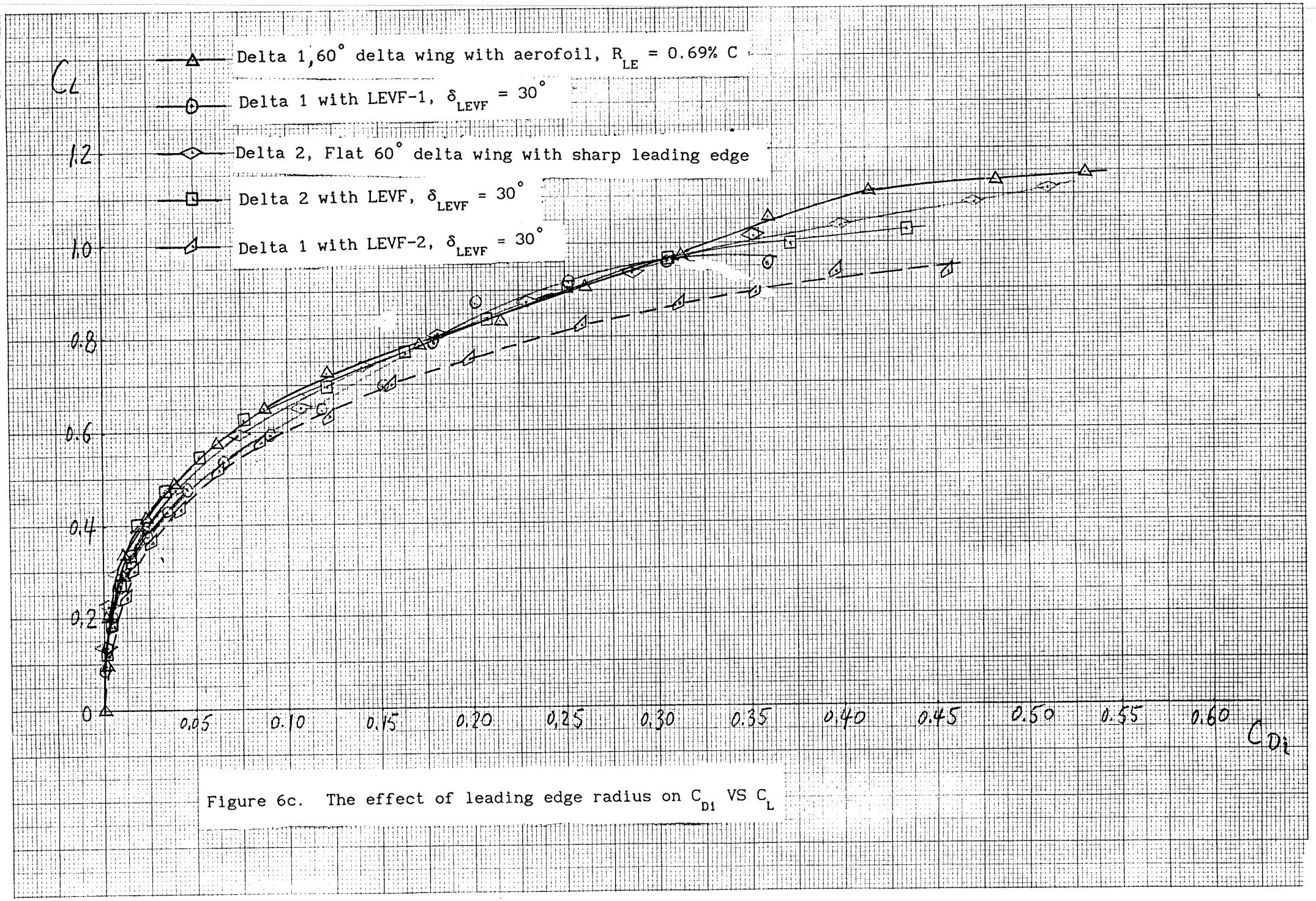

Figure 6c. The effect of leading edge radius on C_{Di} VS C_L

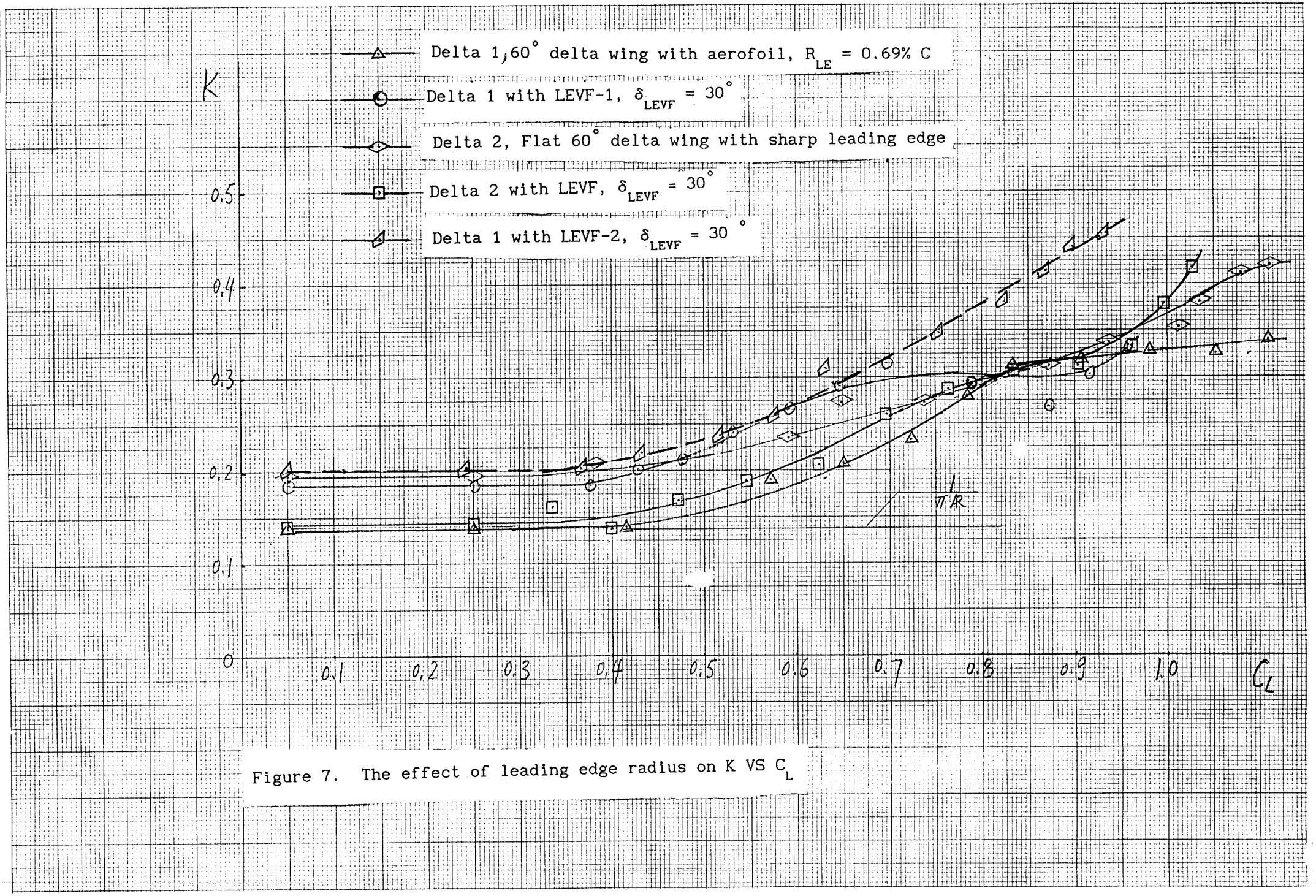

Figure 7. The effect of leading edge radius on K VS C_L

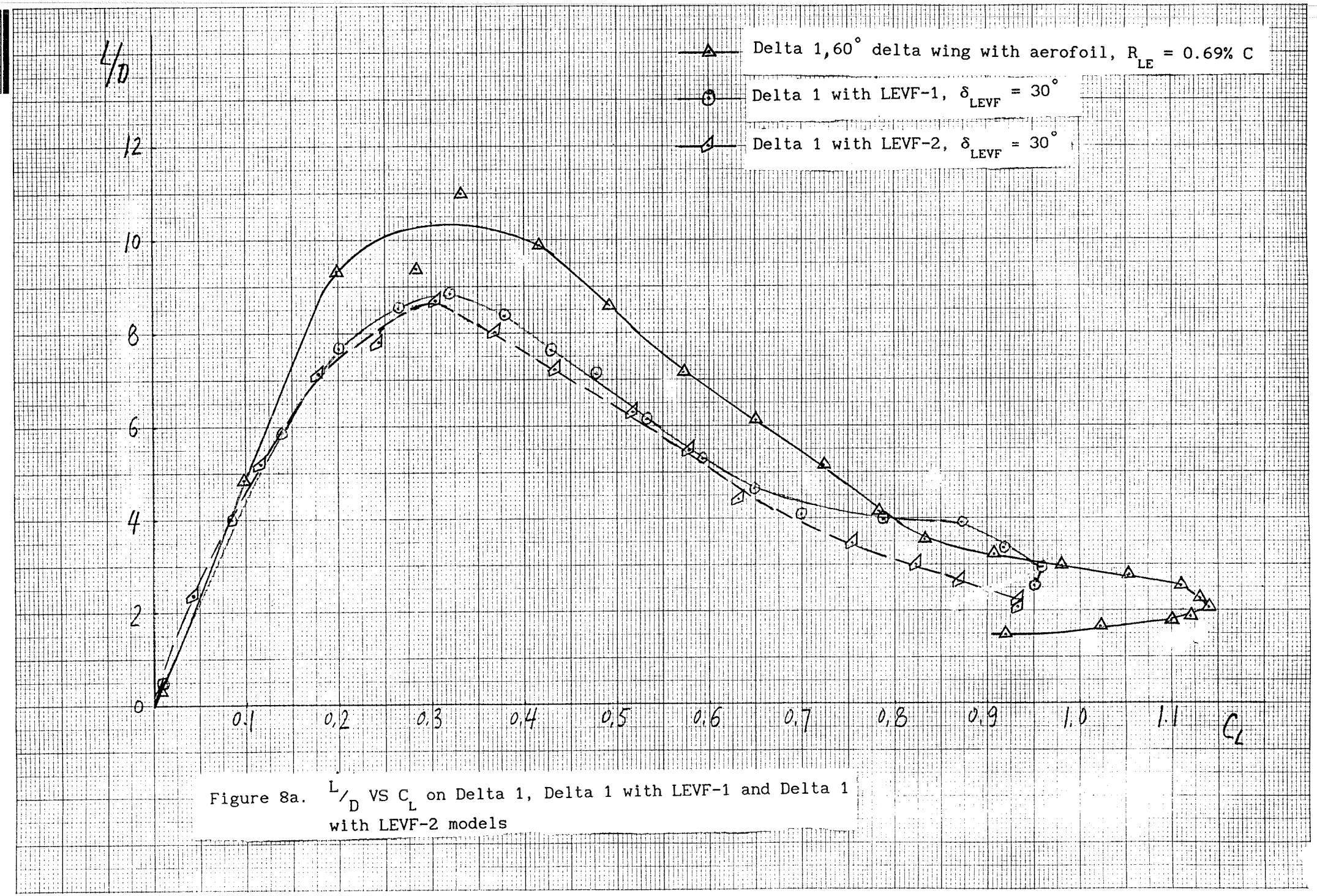

Figure 8a. L/D VS C_L on Delta 1, Delta 1 with LEVF-1 and Delta 1 with LEVF-2 models

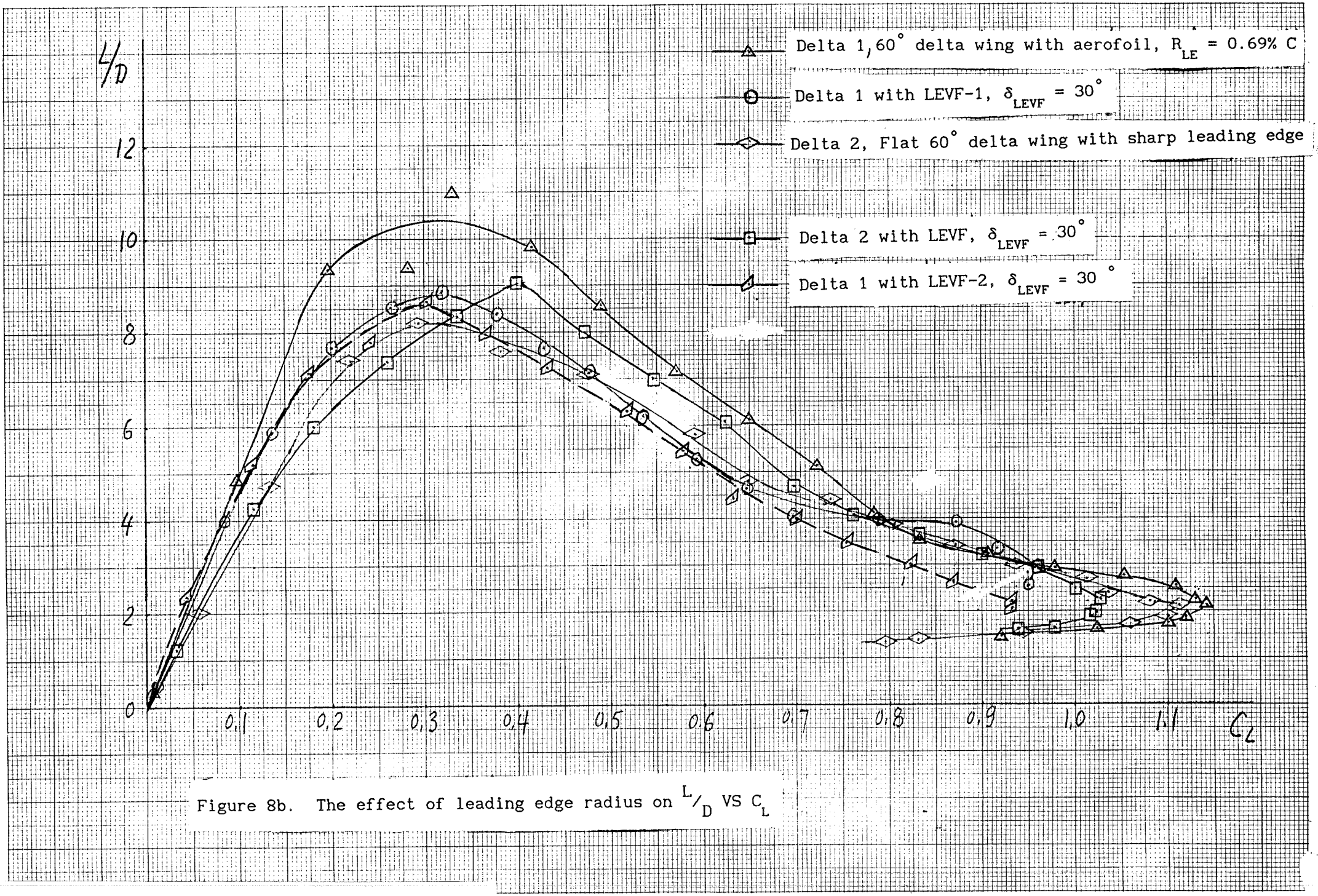

Figure 8b. The effect of leading edge radius on L/D VS C_L